Rate-Induced Transitions and Noise-Driven Resilience in Vegetation Pattern Dynamics

Lilian Vanderveken[1] and Michel Crucifix[1]

[1]Earth and Life Institute, Louvain-la-neuve, Belgium

Correspondence: Lilian Vanderveken (lilian.vanderveken@uclouvain.be)

Abstract. Understanding the resilience and stability of vegetation patterns under changing environmental conditions is crucial for predicting ecosystem responses to climate change. This study investigates the dynamics of vegetation patterns in response to a spatially homogeneous decrease in rainfall across the entire domain. Starting from ~~high-rainfall~~ high rainfall with a stable homogeneous vegetated state, we applied various rates of rainfall reduction to observe system transitions. We find that rainfall

5   decrease may cause transitions to two or three pulse states, or abrupt shifts to bare soil depending on the rate of change, highlighting the significance of rate-induced tipping (R-tipping) in open dynamical systems.

We identified the pulse creation and destruction timescale (τ_{pulse}) and the rearrangement timescale (τ_{rear}) as the critical timescales which govern the system response to gradual environmental changes. The rearrangement timescale, significantly longer than τ_{pulse}, is relevant for ~~characterising the system behavior~~ characterizing the system behaviour under slow perturba-

10   tions. Dimensional analysis and sensitivity analysis with numerical experiments further validate the fundamental connections between these timescales.

Additionally, we examined the impact of spatially and temporally structured noise on vegetation pattern resilience. Perturbations ~~modeled~~ modelled as Gaussian stochastic processes with specific autocorrelation structures were applied to the system. We find that increased spatial autocorrelation in noise reduces pattern formation, while temporal autocorrelation at critical

15   timescales significantly influences biomass mean and variance. The co-existence of multiple equilibria and unstable states, combined with the presence of ghost attractors enhances system resilience by providing alternative stable configurations under fluctuating conditions.

These findings underscore the importance of considering slow timescales and structured noise in analyzing vegetation dynamics. Understanding these factors is essential for predicting ecosystem resilience and developing strategies to manage vege-

20   tation systems under climate variability.

1

1   Introduction

Understanding the dynamics of vegetation patterns under varying environmental conditions is crucial for predicting ecosystem responses to climate change. Vegetation patterns, such as the regular arrangement of plant patches, arise from complex interactions between biological processes and environmental factors (Klausmeier, 1999a). These patterns are particularly sensitive to changes in environmental conditions (Gilad et al., 2007), which directly affect, for example, water availability, a critical resource for plant growth in semi-arid regions (Deblauwe et al., 2008). Therefore, investigating how vegetation systems respond to different perturbations can provide valuable insights into their resilience and stability.

The seminal works by Holling (1973) established the difference, in ecology, between stability and resilience. Stability refers to the ability of a system to return to its equilibrium after a perturbation and is linked to the eigenvalues associated with a given stable equilibrium. Resilience defines the ability of an ecosystem to maintain its function. For example, in semi-arid areas, an ecosystem constrained by limited water supply may achieve its highest biomass when vegetation is distributed in the form of patterns. Furthermore, based on vegetation models, we know that different pattern configurations may be compatible with a same boundary condition (von Hardenberg et al. (2001), Dijkstra (2011), Zelnik et al. (2013)). As these different configurations may all achieve high biomass, it is generally conjectured that resilience is effectively enhanced by the multiplicity of possible patterns.

However, understanding resilience also requires attention to the nature of the perturbation (Kéfi et al., 2019): A system may react very differently depending on the type of perturbation being applied to it.

Our objective is to determine the critical scales, in time and space, which determine the response of the system to environmental perturbations. We consider, at first, linear, deterministic perturbations such as a linear decrease in precipitation, and then stochastic perturbations. We aim at establishing general principles. Even though the work is based on a specific numerical model of vegetation (Rietkerk et al., 2002), we aim at identifying which critical time scales emerge from the model construction, and how they influence the system's response.

To this end, we follow the framework established by previous studies. More specifically, Siteur et al. (2014), Chen et al. (2015) and Sherratt (2013) showed the importance of the rate of change and noise; Bastiaansen et al. (2020) identified in Klausmeier's vegetation patterns model a critical time scale for which the patterns do not have the time to adapt to the environmental change. All those works emphasize the importance of understanding rate-induced transitions.

After those studies, a number of questions remain: are there more than one critical time scale in a vegetation pattern model; what is the impact of those internal timescales, and can they be linked to parameters of the model? In the following, we will show how these critical timescales manifest themselves in Rietkerk's model (Rietkerk et al., 2002), and how they influence both the response to deterministic and stochastic perturbations, with emphasis on the possible occurrence of a resonance process.

2   Model description

As announced in the introduction we use the vegetation model by Rietkerk et al. (2002). As common for reaction-diffusion models, it combines two mechanisms for creating patterns: local facilitation, and long-range inhibition. Local facilitation is caused by the water infiltration feedback. It is based on the idea that in a semi-arid region the soil crust effectively prevents water infiltration. The presence of biomass and more specifically the roots associated with this vegetation increases the water infiltration by drilling the soil crust. Long-range inhibition is caused by rapid diffusion of surface water preventing the accumulation of water in some places of the spatial domain and so the creation of biomass. The presence of these two processes places the Rietkerk's model in the category of scale-dependent feedback model. (Lefever and Lejeune (1997), Rietkerk and van de Koppel (2008), van de Koppel et al. (2005)). Although models of this class are known to produce regular patterns as stable equilibria, Vanderveken et al. (2023) showed that non regular equilibria (Mixed state) exist and play a role in the dynamic of the system despite its instabilities. Another class of pattern-formation models have been proposed recently by Siteur et al. (2023). This class of models is based on density-dependent-aggregation of biotic or abiotic species and can create non regular patterns.

Three variables are modelled in Rietkerk's model: Biomass (B) [$g\,m^{-2}$], soil water (W) [mm] and surface water (O) [mm]. They respond to the following system of partial differential equations:

$$\frac{\partial B}{\partial t} = cg_{max}\frac{W\,B}{W + k_1} - dB + D_B\Delta B,$$

$$\frac{\partial W}{\partial t} = \alpha O\frac{B + k_2 w_0}{B + k_2} - g_{max}\frac{W\,B}{W + k_1} - r_w W + D_W\Delta W,$$

$$\frac{\partial O}{\partial t} = R - \alpha O\frac{B + k_2 w_0}{B + k_2} + D_O\Delta O, \tag{1}$$

where Δ is the Laplacian operator and R the rainfall [$mm.d^{-1}$]. Rainfall is the external forcing of the system which we consider to be a spatially-independent function. The first term in the biomass equation represents water uptake by the plant. The first term in the soil water equation is linked to the infiltration rate of water in the soil that is enhanced by the presence of biomass. The factors in front of the Laplacians (ΔB, ΔW and ΔO) represent the diffusion constants of the different quantities. We consider a periodic domain of size $l = 100$m. The parameters are provided in appendix A.

3   Effect of Rainfall Perturbation on Vegetation Dynamics: Identifying Critical Timescales

We consider a spatially homogeneous perturbation applied to surface water, representing a decrease in rainfall across the entire domain. This type of perturbation is meaningful as it mimics scenarios of prolonged droughts or gradual shifts in climate patterns. By applying different rates of change to a system that is initially in a high rainfall state, we aim at identifying which critical factors influence the transient response of vegetation.

Previous research has highlighted the dependence of system solutions on the rate of environmental change, as common in open dynamical systems. In the context of vegetation patterns, different rates of rainfall decrease can lead to diverse outcomes, ranging from transitions to multi-pulse states to abrupt shifts to bare soil.

Starting from a high rainfall situation ($R = 1.4\text{mm.day}^{-1}$ ~~$R = 1.4\text{mm.day}^{-1}$~~ $R = 1.4\,\text{mm}\,\text{day}^{-1}$), for which only the homogeneous vegetated state is stable, we decrease rainfall with different rates of change a (~~[mm.day^{-2}]~~ [$\text{mm}\,\text{day}^{-2}$]). Figure 1 shows the evolution of the spatial structure of the biomass (in green) as a function of rainfall, for different values of a. We find a transition from an homogeneous state to a heterogeneous distribution with two or three vegetation 'pulses', before it finally disappears. The sequence and timing of the transitions depend on a. For a rate of change of ~~$10^{-3}\,\text{mm.day}^{-2}$~~ $10^{-3}\,\text{mm}\,\text{day}^{-2}$ the system jumps directly from a homogeneous vegetated state to a bare soil solution. The critical rate of change at which all vegetation is eradicated is $\tau_{R_{\text{tip}}} \sim 1000$ days.

The existence of multistability implies hysteresis behaviour. When reversing the rainfall gradient—from low to high—the system takes a different paths for the transition between low and high biomass.

It is not surprising that the response depends on the rate of the perturbation change. Ashwin et al. (2012) established general principles of so-called rate-induced tipping (R-tipping) in models based on ordinary differential equations, and rate-dependent response were also described specifically in models of vegetation patterns (Siteur et al. (2014), Chen et al. (2015), Bastiaansen et al. (2020)). However, the value of $\tau_{R_{\text{tip}}}$ is intriguing. Indeed, the timescale associated with the destruction and creation of vegetation pulses is, through dimensional analysis, estimated to be $\tau_{\text{pulse}} = \frac{c}{k_2}\frac{R}{r_w}\frac{1}{d} = 30\text{days}$. It is ~~is~~ linked to the transfer of water to the biomass and to the destruction of the vegetation.

Having $\tau_{R_{\text{tip}}}$ about 30 times τ_{pulse} suggests that a slower process dominates the system's ~~behavior~~ behaviour under changing environmental conditions. Bastiaansen et al. (2020) already identified another critical timescale within the Klausmeier's model (Klausmeier (1999b)). It is linked to the movement of pulses towards a stable, regular state. This concept is crucial for understanding vegetation dynamics in response to gradual environmental changes.

We now proceed to determine a similar time scale in Rietkerk et al. (2002)'s model, and will call it the rearrangement timescale, τ_{rear}.

First, we perform a numerical experiment where a pulse is removed for a given rainfall value, and the time taken for the system to stabilize is computed. Figure 2 shows the results for different values of rainfall. We find that $\tau_{\text{rear}} \sim 1000$ days. This rearrangement timescale is of the same order as $\tau_{R_{\text{tip}}}$, suggesting a fundamental connection between the two. This correspondence would also support that R-tipping is conditioned by the slowest timescale in the system. The rearrangement timescale effectively represents this slowest process, dictating the system's overall response to changing conditions. ~~We now~~ Second, we attempt to link this rearrangement timescale to quantities in the system. Inspired by the scaling proposed in Bastiaansen and Doelman (2019), we reason on the fact that the movement of pulses are determined by diffusion coefficients. Specifically, we take the advantage of the fact that the ratio between the slow and the fast diffusion coefficients in the reaction-diffusion model drives the creation of the patterns (Murray (2003),Meron (2015)). For Rietkerk's model the fast component is the surface water (O) and the slow components are the biomass (B) and the soil water (W). Hence, we propose the following scaling for the rearrangement time $\tau_{rear} = \frac{c}{k_2}\frac{R}{r_w}\frac{1}{d}\sqrt{\frac{D_O}{D_B}} = 1000\text{d}$. The key factor determining the rearrangement time appears to be the square root of the ratio between the diffusion coefficients of the fast and slow variables. To verify this, we perform a series of experiments where the diffusion coefficient of the slow variables (biomass and soil water) varied by a factor f. To obtain a ~~stabilisation~~ stabilization time for the different values of f, we run a series of numerical experiments similar to the one

4

presented earlier. We start from a stable state for a given value of rainfall and f, then we remove one pulse of vegetation. We compute this ~~stabilisation~~ stabilization time for different values of rainfall and took the larger ~~stabilisation~~ stabilization time because it is the one that is of interest regarding R-tipping. The results are presented in Figure ~~2~~3. The rearrangement ~~time scale~~ timescale which is diagnosed numerically fits the theoretical curve proposed for τ_{rear} fairly well.

This finding highlights the critical role of the rearrangement timescale in determining the system's response to environmental changes. Specifically, it emphasizes the need to account for this slower timescale when analyzing vegetation dynamics. Understanding and quantifying this timescale provides valuable insights into the resilience and stability of vegetation systems under gradual environmental shifts.

4 Effect of Spatially and Temporally Structured Noise on Vegetation Pattern Resilience

The kind of perturbations applied to the system is an important aspect of resilience diagnosis (Kéfi et al. (2019)) and specifically, the spatial scale of the perturbation must be considered. In the following section, we consider a dynamic perturbation consisting of a spatially distributed noise modeled mathematically as a Gaussian stochastic process with mean $\mathbb{E}[\xi(t,x)] = 0$ and standard deviation $\sigma = 0.1$. The temporal structure is that of an Orstein-Uhlenbeck process. The correlation function is $\mathbb{E}[\xi(t,x)\xi(s,y)] = e^{-|t-s|/\lambda_t} e^{-(x-y)^2/\lambda_s^2}$.

Stochastic perturbations are applied to the biomass B and surface water W. Formally, the model takes the form of:

$$\frac{\partial B}{\partial t} = cg_{max}\frac{W\,B}{W + k_1} - dB + D_B\Delta B + \xi_B(x,t),$$
$$\frac{\partial W}{\partial t} = \alpha O\frac{B + k_2 w_0}{B + k_2} - g_{max}\frac{W\,B}{W + k_1} - r_w W + D_W\Delta W,$$
$$\frac{\partial O}{\partial t} = R - \alpha O\frac{B + k_2 w_0}{B + k_2} + D_O\Delta O + \xi_O(x,t). \tag{2}$$

where $\xi_O(x,t)$ and $\xi_B(x,t)$ are independent noise processes. For biomass, we consider an autocorrelation timescale of one day, and different autocorrelation length-scales ($\lambda_{biomass,s}$) are tested. For surface water, the perturbation is homogeneous in space ~~, in different autocorrelation time-scales~~ and different autocorrelation timescales $\lambda_{rainfall,t}$ are tested.

Figure 4 ~~summarises~~ summarizes the stationary response of the model to $\lambda_{biomass,s}$ and $\lambda_{rainfall,t}$, considering the mean biomass. Outputs reported on those tables is the average of 15 experiments. First, we consider the spatial structure of the noise, applied to the biomass. ~~That is, we~~ We focus on the horizontal lines of the tables, one by one, with the structure of the perturbation changing from highly heterogeneous to almost homogeneous as each line is browsed from the left to the right (increasing $\lambda_{biomass,s}$) We find that mean biomass tends to decrease as spatial autocorrelation increases, and this occurs regardless of the choice of time autocorrelation. This suggests that more homogeneous stochastic perturbations tend to destroy more biomass and send the system towards the bare soil equilibrium. The resilience of the vegetation is thus reduced if the perturbation is spatially more homogeneous.

~~We~~ Second, we now focus on the time-correlation of the stochastic perturbation of surface water. We find that both the spatial mean *and* the variance reach a minimum at $\lambda_t = 10d$. This timescale is the τ_{pulse} timescale previously identified by the scale

analysis. This suggests a form of resonance associated with τ_{pulse} preventing self-organisation of vegetation. On the other hand, biomass reaches a maximum for a perturbation time scale of 1000 days, coinciding with the rearrangement timescale τ_{rear} that we also identified by the scaling analysis.

To visualise the behavior for those different values of temporal autocorrelation, we show, in Figure 5, realizations representative of the general behavior, for four values of λ_t. We see that patterns tend to disappear for $\lambda_t = 10$d and reappear for $\lambda_t = 1000$d. The ability of the system to maintain or not patterns, depending on the time scale of the perturbation, explains the variation of mean biomass observed in Figure 4. We suggest that the slow stochastic perturbation is more effective at moving the system gently around the states associated with the highest biomass, without destroying patterns. The slow timescale (rearrangement timescale) is intrinsically linked to the spatial extension of the model. It would not exist in a zero-dimensional analysis. In this respect, we have noted already that nonlinear, spatially extended systems tend to have multiple equilibria for a given input, here, a given rainfall. The multiplicity of equilibria, whether they are stable or not, increases the resilience of the system in the sense of Holling (1973). Metaphorically, such equilibria may be seen as tree branches in a forest to which an orangutan might cling to avoid falling. This phenomenon is clearly visible in Figure 6, displaying the time evolution of the biomass with a fixed rain fall of $0.8\text{mm}\,\text{d}^{-1}$. In this configuration, we see that the system jumps from a pulse configuration to an other, passing from two to three pulses or vice versa. The transition, associated with the vanishing or the creation of a pulse, happens quickly, with a time scales of a few days. We find again the τ_{pulse} (fast) timescale identified earlier. Those configurations correspond to stable equilibria for the chosen rainfall as previously identified (Zelnik et al. (2013), Vanderveken et al. (2023)). The two and three pulse configurations are not the only states being visited by the system. From time to time a big pulse associated with a small pulse configuration appears. The latter does not correspond to an equilibrium for a rainfall value of 0.8mmd^{-1}, but it can be interpreted as the ghost of a *mixed state* identified in Vanderveken et al. (2023). Mixed states are always unstable and exhibit pulses with different heights. The mixed state that interests us here is the one with one big pulse and one small pulse. Its existence spans from 0.6mmd^{-1} to less than 0.8mmd^{-1}. In the stochastic realization, the position of the second small pulse is not perfect because of noise. We clearly see that even if this mixed state with two pulses is not an equilibrium for this value of rainfall, it plays a role in the dynamics, hence the qualifier of "ghost" (Hastings et al. (2018) and Morozov et al. (2020)). Ghost attractors and unstable equilibria expand the resilience of the system because, in view of the orangutan in the forest, these configurations are new tree branches to cling to.

In this study, we focused on the effect of spatial and temporal correlations on the system. To assess the impact of noise amplitude, we performed numerical experiments for low noise intensity $\sigma = 0.09$ and high noise intensity levels, $\sigma = 0.3$ and $\sigma = 0.9$. We observed that the results are consistent for low value of noise amplitude.

For $\sigma = 0.3$, we observe pattern destruction at $\lambda_t = 1$d, followed by pattern reappearance at higher values of temporal autocorrelation. At $\sigma = 0.9$, all patterns are destroyed, and the system stabilizes into a spatially homogeneous solution oscillating with rainfall.

Regarding mean biomass, we observed for both $\sigma = 0.3$ and $\sigma = 0.9$, a consistent increase with increasing temporal autocorrelation. This behaviour can be understood by two complementary numerical experiments.

First, we applied noise exclusively to the surface water, using three values of $\sigma = 0.1, 0.3, \text{and} 0.9$. For $\sigma = 0.1$, biomass is eliminated at $\lambda_t = 10$d. For higher noise amplitudes, two phenomena emerge: (1) the range of temporal autocorrelation over which biomass is reduced shifts to lower values of λ_t, and (2) the mean biomass increases significantly at higher λ_t. Together, these effects result in an increase in biomass with increasing temporal autocorrelation.

Second, we applied noise exclusively to the biomass components, using the same three values of σ and fixing temporal autocorrelation at $\lambda_t = 1$d. In this setup, we observe that mean biomass increases with σ. This can be attributed to the nature of the Gaussian noise applied. Gaussian noise is symmetric, and since biomass is constrained to be non-negative, the system benefits more from the positive phases of the noise while being less affected by the negative phases. As the amplitude of the noise increases, this asymmetry leads to an overall increase in biomass.

The combined effects of noise applied to both surface water and biomass explain the observed increase in mean biomass for $\sigma > 0.1$. However, the destruction and reappearance of patterns remain robust even at higher noise amplitudes (e.g., $\sigma = 0.3$). At sufficiently high noise intensity ($\sigma = 0.9$), a saturation effect occurs, and the system becomes entirely noise-driven, with patterns fully suppressed.

By demonstrating that resilience is bolstered by spatially heterogeneous noise and identifying critical timescales that influence biomass dynamics, we have provided valuable insights into the mechanisms underpinning ecological stability. Our findings emphasize the necessity of considering both stable and metastable states in resilience assessments, offering a more comprehensive understanding of ecosystem dynamics under varying perturbation regimes.

5 Conclusions

The present study explored the effects of a spatially homogeneous perturbation, specifically a decrease in rainfall, on vegetation dynamics in a model system. By varying the rate of change in rainfall, we observed significant differences in the system's response. At slower rates, the system transitions through multiple stable states, including two and three pulse solutions. However, a critical rate of change at $10^{-3}, \text{mm.d}^{-2}$ results in a direct shift from a homogeneous vegetated state to bare soil. This critical rate of change aligns with a critical timescale $\tau_{R_{\text{tip}}} \sim 1000$ d, much longer than the pulse creation and destruction timescale $\tau_{\text{pulse}} = 30$d, highlighting the dominance of slower processes in the system's ~~behavior~~ behaviour under environmental changes.

5.1 Rearrangement Timescale and System Resilience

We identified a critical rearrangement timescale $\tau_{\text{rear}} \sim 1000$ d, which corresponds to the system's response time to structural changes, such as the removal of a vegetation pulse. This timescale is pivotal for understanding the resilience and stability of vegetation patterns. By linking τ_{rear} to the diffusion coefficients of the system's components, we derived a scaling law that accurately predicts the rearrangement time, emphasizing the importance of spatial interactions in determining system dynamics.

7

5.2 Impact of Spatial and Temporal Noise

We further investigated the resilience of the system under spatial and temporal noise, modeled as Gaussian stochastic processes. The experiments demonstrated that the spatial autocorrelation of noise significantly impacts pattern formation. Higher spatial correlation lead to reduced spatial variance and biomass, suggesting that more homogeneous noise disrupts vegetation patterns. Temporal noise analysis revealed critical timescales—particularly around 10 days and 1000 days—corresponding respectively to the pulse and rearrangement timescales~~, respectively~~. These findings underscore the intricate balance between spatial and temporal scales in maintaining vegetation resilience.

5.3 Broader Implications and Multiple Equilibria

Our analysis highlights the existence of multiple equilibria and the crucial role of slow timescales in spatially extended systems. The presence of ghost attractors and unstable equilibria broadens the system's resilience, offering additional configurations for the system to cling to, akin to tree branches in a forest. This multiplicity of stable and transient states enhances the system's capacity to adapt to gradual environmental changes, aligning with the concept of resilience as defined by Holling (1973).

In summary, this study contributes to ~~elucidate~~ clarify a complex interplay between rainfall perturbations, spatial and temporal noise, and vegetation dynamics. By identifying critical timescales and exploring the system's response to various perturbations, we provide valuable insights into the resilience and stability of vegetation systems. These findings contribute to a deeper understanding of ecological dynamics and the factors influencing the persistence of vegetation patterns under changing environmental conditions.

Code availability. All the code used to produce the figures for this paper is available here: https://zenodo.org/doi/10.5281/zenodo.13739303 (Vanderveken, 2024)

Appendix A: Model parameters

The parameters are as in Rietkerk et al. (2002), see table A1

Appendix B: Structured noise

The noise used in this paper is correlated both in time and space. We prescribe its standard deviation σ, length of spatial autocorrelation λ_s and time correlation λ_t with a period of L. To produce this noise, first, we computed the square root of the following covariance matrix where $N = 100$ is the number of spatial points.

$$\mathbf{A}_{i,j} = max\left(e^{\frac{-(x_i - x_j)^2}{\lambda_s^2}}, e^{\frac{-(L - |x_i - x_j|)^2}{\lambda_s^2}} \right)$$

c	Conversion of water uptake by plants to plant growth	$10\,\mathrm{g\,mm^{-1}\,m^{-2}}$
g_{max}	Maximum water uptake	$0.05\,\mathrm{mm\,g^{-1}\,m^{-2}\,d^{-1}}$
k_1	Half-saturation constant of specific plant growth and water uptake	$5\,\mathrm{mm}$
D_B	Plant dispersal	$0.1\,\mathrm{m^2\,d^{-1}}$
α	Maximum infiltration rate	$0.2\,\mathrm{d^{-1}}$
k_2	Saturation constant of water infiltration	$5\,\mathrm{g\,m^{-2}}$
w_0	Water infiltration in the absence of plants	0.2
r_w	Soil water loss due to evaporation and drainage	$0.2\,\mathrm{d^{-1}}$
D_W	Diffusion coefficient for soil water	$0.1\,\mathrm{m^2\,d^{-1}}$
D_O	Diffusion coefficient for surface water	$100\,\mathrm{m^2\,d^{-1}}$
d	Plant mortality rate	$0.25\,\mathrm{d^{-1}}$

Table A1. Parameters for Rietkerk's model

Then we use an AR1 process in time to create the time dependence of the noise

$$x_{i,j} = x_{i,j} + (-c * x_{i,j}dt + \sqrt{dt}\sigma_e \sum_{k=1}^{n} \mathbf{A}_{j,k}\epsilon_k)$$

with $c = 1/\lambda_t$, dt the time step, $\sigma_e = \sigma\sqrt{2c}$ and ϵ_k a Gaussian random variable of zero mean and variance one.

The resulting noise is exemplified if in A1 and the temporal and spatial structure are shown in A2.

Author contributions. LV and MC designed the study. LV performed the numerical analysis. LV wrote the paper, and MC reviewed and edited the paper

References

240   Ashwin, P., Wieczorek, S., Vitolo, R., and Cox, P.: Tipping points in open systems: Bifurcation, noise-induced and rate-dependent examples in the climate system, Philosophical Transactions of the Royal Society A: Mathematical, Physical and Engineering Sciences, 370, 1166–1184, https://doi.org/10.1098/rsta.2011.0306, 2012.

Bastiaansen, R. and Doelman, A.: The dynamics of disappearing pulses in a singularly perturbed reaction–diffusion system with parameters that vary in time and space, Physica D: Nonlinear Phenomena, 388, 45–72, https://doi.org/10.1016/j.physd.2018.09.003, 2019.

245   Bastiaansen, R., Doelman, A., Eppinga, M. B., and Rietkerk, M.: The effect of climate change on the resilience of ecosystems with adaptive spatial pattern formation, Ecology Letters, 23, 414–429, https://doi.org/10.1111/ele.13449, 2020.

Chen, Y., Kolokolnikov, T., Tzou, J., and Gai, C.: Patterned vegetation, tipping points, and the rate of climate change, European Journal of Applied Mathematics, 26, 945–958, https://doi.org/10.1017/S0956792515000261, 2015.

Deblauwe, V., Barbier, N., Couteron, P., Lejeune, O., and Bogaert, J.: The global biogeography of semi-arid periodic vegetation patterns,
250   Global Ecology and Biogeography, 17, 715–723, https://doi.org/10.1111/j.1466-8238.2008.00413.x, 2008.

Dijkstra, H. A.: Vegetation pattern formation in a semi-arid climate, International Journal of Bifurcation and Chaos, 21, 3497–3509, https://doi.org/10.1142/S0218127411030696, 2011.

Gilad, E., von Hardenberg, J., Provenzale, A., Shachak, M., and Meron, E.: A mathematical model of plants as ecosystem engineers, Journal of Theoretical Biology, 244, 680–691, https://doi.org/10.1016/j.jtbi.2006.08.006, 2007.

255   Hastings, A., Abbott, K. C., Cuddington, K., Francis, T., Gellner, G., Lai, Y. C., Morozov, A., Petrovskii, S., Scranton, K., and Zeeman, M. L.: Transient phenomena in ecology, Science, 361, https://doi.org/10.1126/science.aat6412, 2018.

Holling, C. S.: Resilience and Stability of Ecological Systems, Annual Review of Ecology and Systematics, 4, 1–23, http://www.jstor.org/stable/2096802, 1973.

Kéfi, S., Domínguez-García, V., Donohue, I., Fontaine, C., Thébault, E., and Dakos, V.: Advancing our understanding of ecological stability,
260   Ecology Letters, 22, 1349–1356, https://doi.org/10.1111/ele.13340, 2019.

Klausmeier, C. A.: Regular and Irregular Patterns in Semiarid Vegetation, Science, 284, 1826–1828, https://doi.org/10.1126/science.284.5421.1826, 1999a.

Klausmeier, C. A.: Regular and irregular patterns in semiarid vegetation, Science, 284, 1826–1828, https://doi.org/10.1126/science.284.5421.1826, 1999b.

265   Lefever, R. and Lejeune, O.: On the origin of tiger bush, Bulletin of Mathematical Biology, 59, 263–294, https://doi.org/10.1007/BF02462004, 1997.

Meron, E.: Nonlinear physics of ecosystems, CRC Press, ISBN 9781439826324, https://doi.org/10.1201/b18360, 2015.

Morozov, A., Abbott, K., Cuddington, K., Francis, T., Gellner, G., Hastings, A., Lai, Y. C., Petrovskii, S., Scranton, K., and Zeeman, M. L.: Long transients in ecology: Theory and applications, Physics of life reviews, 32, 1–40, https://doi.org/10.1016/j.plrev.2019.09.004, 2020.

270   Murray, J. D.: Mathematical Biology II : Spatial Models and Biomedical Applications , Third Edition, Springer New York, NY, ISBN 0387952284, 2003.

Rietkerk, M. and van de Koppel, J.: Regular pattern formation in real ecosystems, Trends in Ecology and Evolution, 23, 169–175, https://doi.org/10.1016/j.tree.2007.10.013, 2008.

Rietkerk, M., Boerlijst, M. C., van Langevelde, F., HilleRisLambers, R., van de Koppel, J., Kumar, L., Prins, H. H. T., and de Roos, A. M.:
275   Self-Organization of Vegetation in Arid Ecosystems, The American Naturalist, 160, 524–530, https://doi.org/10.1086/342078, 2002.

Sherratt, J. A.: History-dependent patterns of whole ecosystems, Ecological Complexity, 14, 8–20, https://doi.org/10.1016/j.ecocom.2012.12.002, 2013.

Siteur, K., Siero, E., Eppinga, M. B., Rademacher, J. D., Doelman, A., and Rietkerk, M.: Beyond Turing: The response of patterned ecosystems to environmental change, Ecological Complexity, https://doi.org/10.1016/j.ecocom.2014.09.002, 2014.

280 Siteur, K., Liu, Q.-X., Rottschäfer, V., van der Heide, T., Rietkerk, M., Doelman, A., Boström, C., and van de Koppel, J.: Phase-separation physics underlies new theory for the resilience of patchy ecosystems, Proceedings of the National Academy of Sciences, 120, 2017, https://doi.org/10.1073/pnas.2202683120, 2023.

van de Koppel, J., Rietkerk, M., Dankers, N., and Herman, P. M.: Scale-dependent feedback and regular spatial patterns in young mussel beds., The American naturalist, 165, https://doi.org/10.1086/428362, 2005.

285 Vanderveken, L.: Stochastic Rietkerk model, https://doi.org/10.5281/zenodo.13739304, 2024.

Vanderveken, L., Martínez Montero, M., and Crucifix, M.: Existence and influence of mixed states in a model of vegetation patterns, Nonlinear Processes in Geophysics, 30, 585–599, https://doi.org/10.5194/npg-30-585-2023, 2023.

von Hardenberg, J., Meron, E., Shachak, M., and Zarmi, Y.: Diversity of vegetation patterns and desertification, Physical Review Letters, 87, 198 101–1–198 101–4, https://doi.org/10.1103/PhysRevLett.87.198101, 2001.

290 Zelnik, Y. R., Kinast, S., Yizhaq, H., Bel, G., and Meron, E.: Regime shifts in models of dryland vegetation, Philosophical Transactions of the Royal Society A: Mathematical, Physical and Engineering Sciences, 371, https://doi.org/10.1098/rsta.2012.0358, 2013.
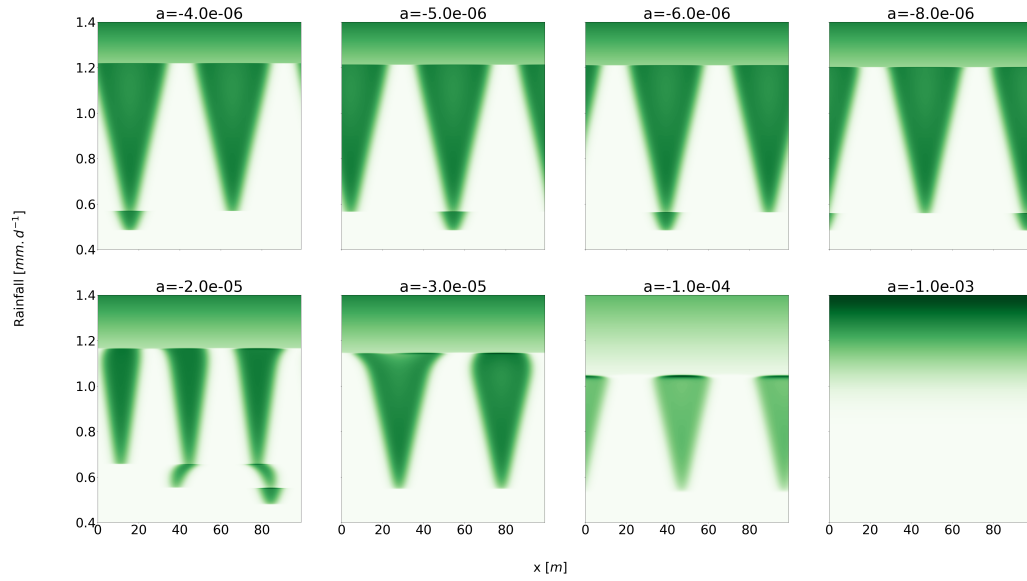
Figure 1. Sensitivity of Rietkerk's model to various rates of change in the rainfall. Each panel represents a solution with a given rate of change a. The x-axis is the spatial dimension, and y-axis the rainfall. Every run has the same starting and ending point rainfall values but they differ by the rate of change. Every simulation starts with a homogeneous vegetated state which is the only stable equilibrium at this value of rainfall. For the last value of rainfall ($R = 0.4\,\mathrm{mm\,days^{-1}}$), the only stable equilibrium is the homogeneous bare soil solution.
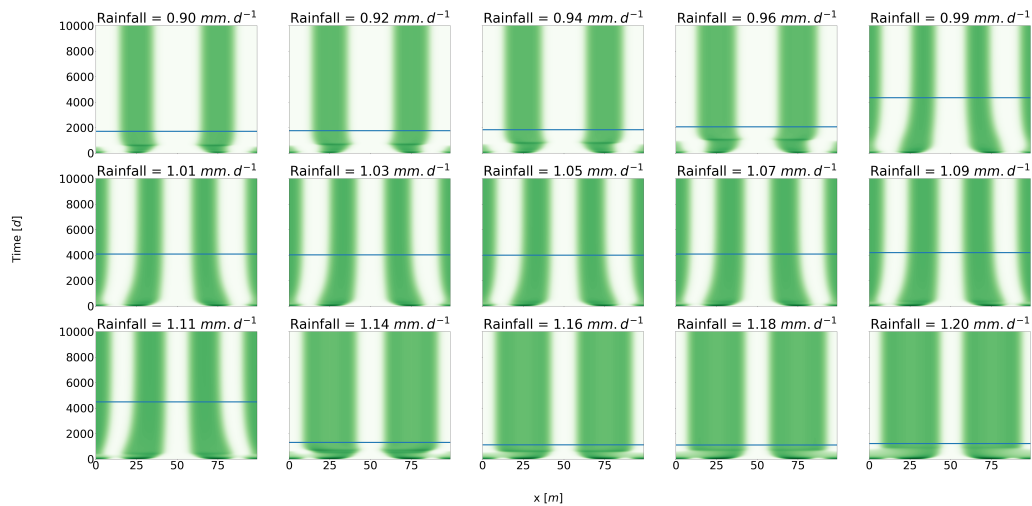
Figure 2. Rearrangement time scale with respect to the rainfall. Each panel represents the solution of the following numerical experiments, we start in the stable equilibrium with four pulses and we remove one pulse. We then identify for each experiment the time until the system reaches a new equilibrium by moving around the pulses. This time is shown by a horizontal blue line on each panel.
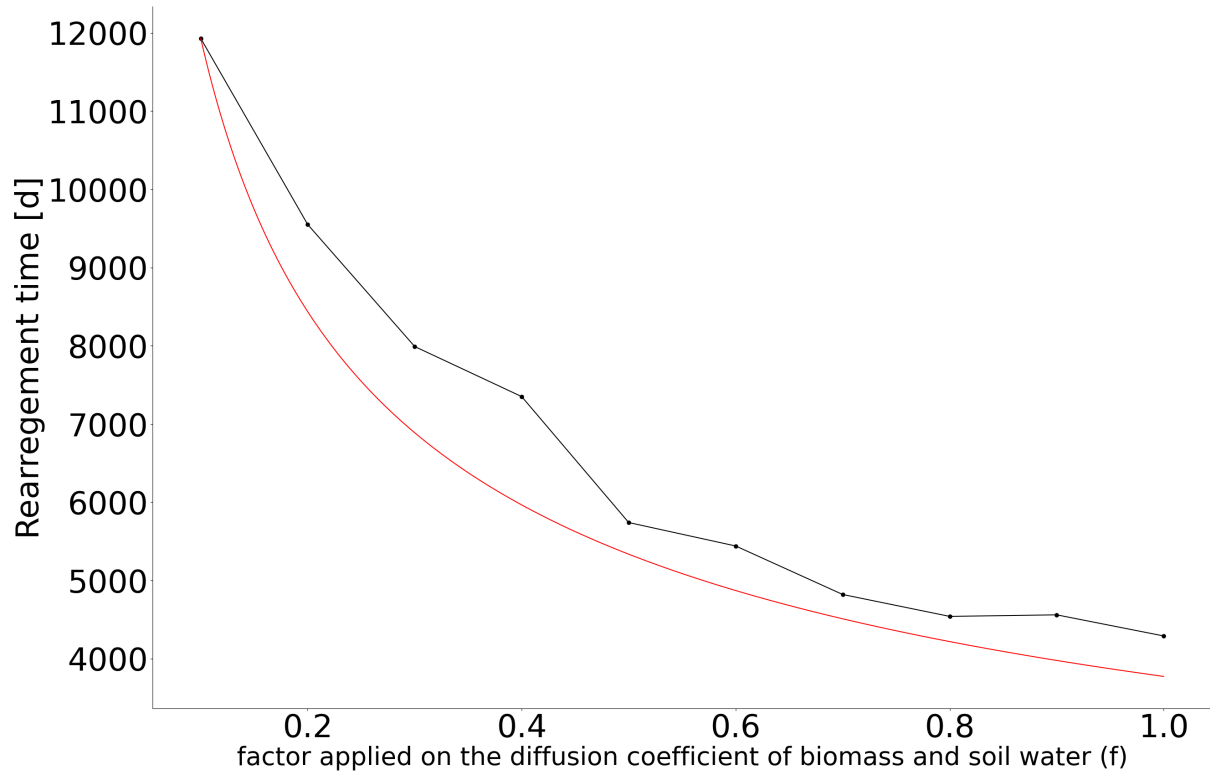
Figure 3. Link between the factor f applied on the diffusion coefficient of the the "slow" components (biomass and soil water) and the rearrangement timescale. This timescale is estimated by finding a stable equilibrium for the new diffusion coefficients, remove one of the pulse and then estimate the ~~stabilisation~~ stabilization time. This procedure is applied for different values of rainfall and we take into account the largest ~~stabilisation~~ stabilization time. The results are the black dot and the red line scales as $\frac{1}{\sqrt{x}}$

Figure 4. Summary table for the runs with stochastic forcing. For each cell, we ran the model 15 times with the same λ_t and λ_s. The table indicates the ensemble mean of the temporal mean of the spatial mean.
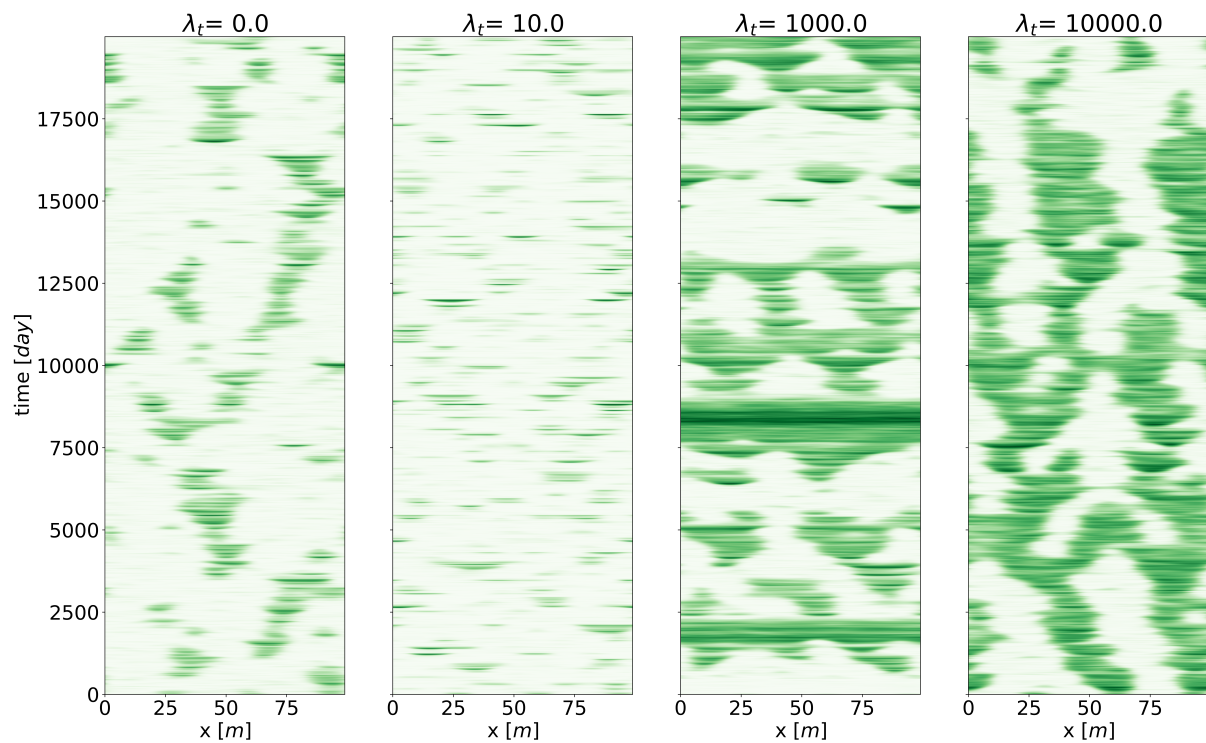
Figure 5. Four ~~realisations~~ realizations of the stochastic Rietkerk model with $\lambda_s = 1$m. The biomass is the variable shown. Each panel shows a representative ~~realisation~~ realization with different temporal autocorrelations (λ_t).
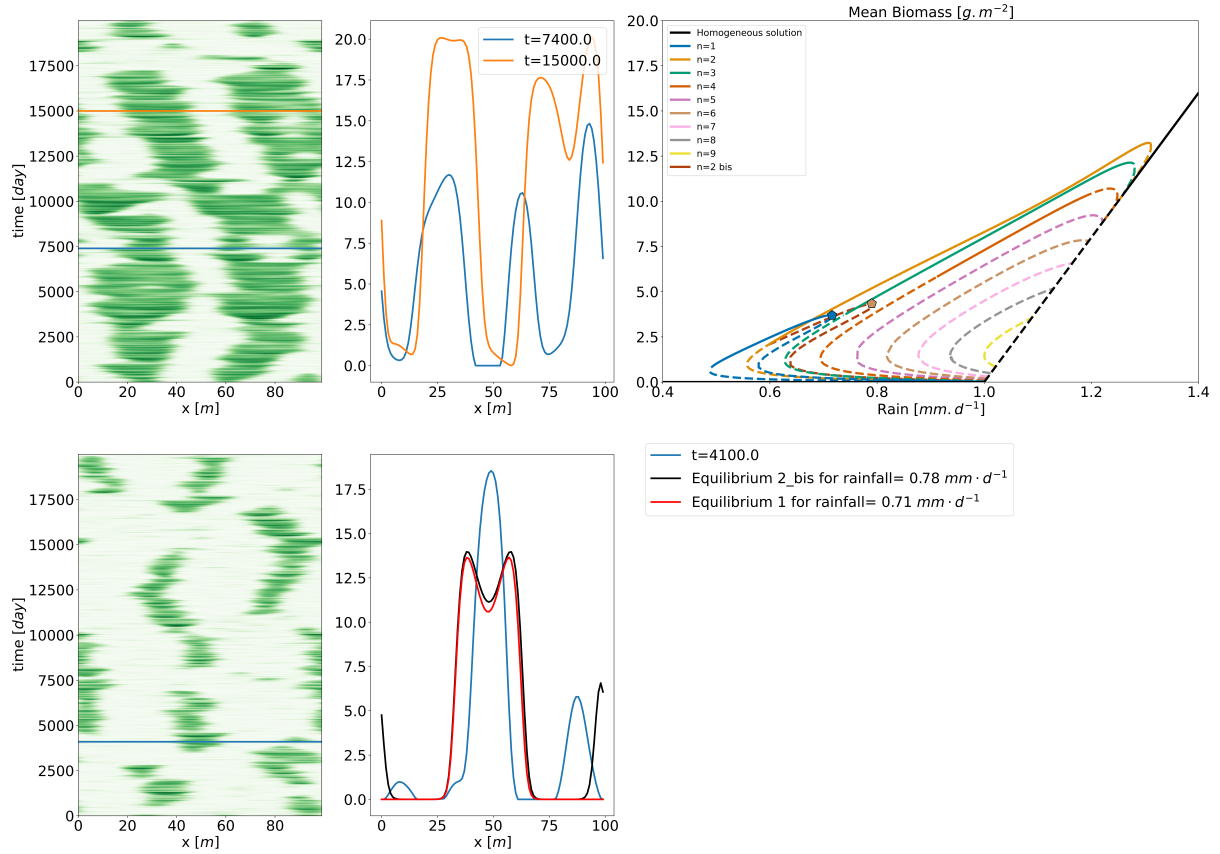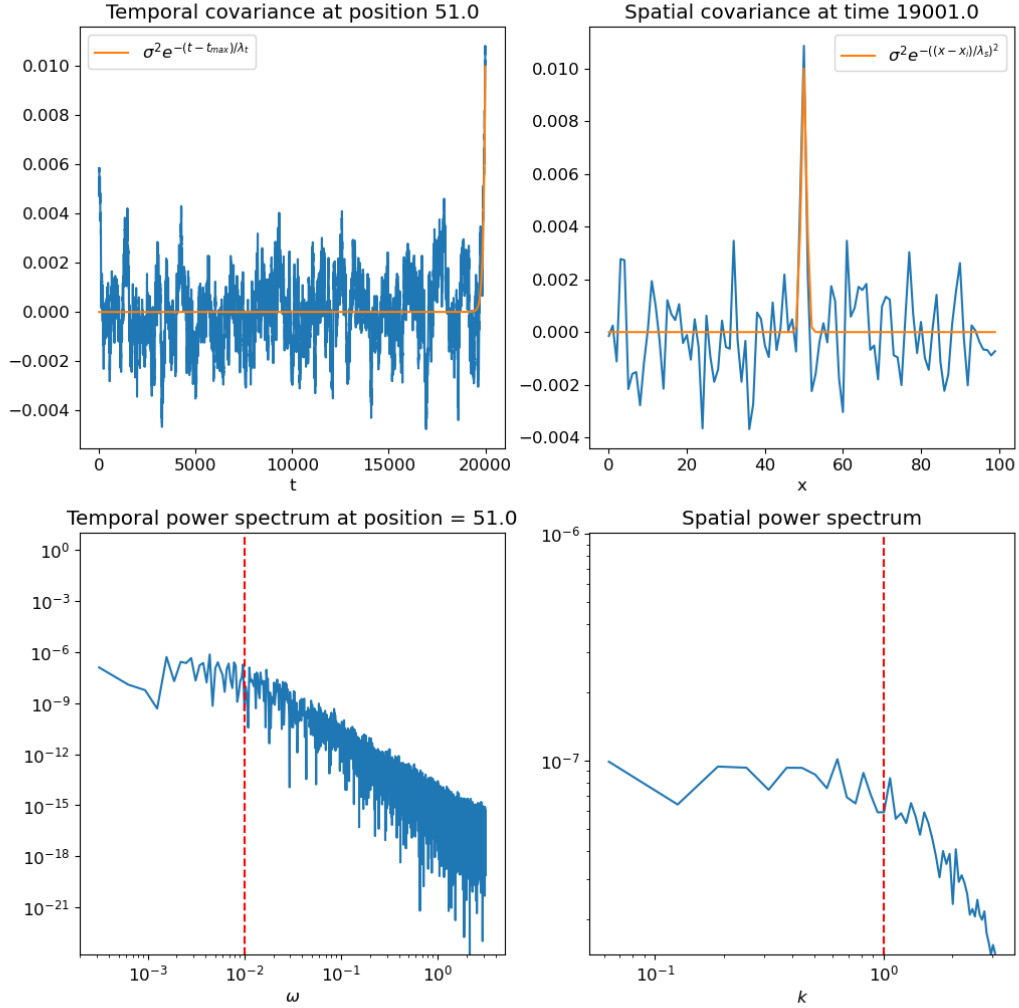
Figure 6. Two ~~realisations~~ realizations of the stochastic Rietkerk model with different noises. On the top-left panel, the parameters are ~~$R = 0.8\,\mathrm{mmd}^{-1}$~~ $R = 0.8\,\mathrm{mm\,d}^{-1}$, $\lambda_t = 1\mathrm{d}$ and $\lambda_s = 10\mathrm{m}$ for the noise applied on the biomass, and $\lambda_t = 10000\mathrm{d}$ and spatially homogeneous for the noise applied on the surface water. On the ~~top-bottom~~ bottom-left panel, the parameters are ~~$R = 0.8\,\mathrm{mmd}^{-1}$~~ $R = 0.8\,\mathrm{mm\,d}^{-1}$, $\lambda_t = 1\mathrm{d}$ and $\lambda_s = 15\mathrm{m}$ for the noise applied on the biomass, and $\lambda_t = 1\mathrm{d}$ and spatially homogeneous for the noise applied on the surface water. The three horizontal lines mark the timing of the snapshots represented on the ~~right~~ middle panels respectively. The top-right panel gives the bifurcation diagram with two pentagons marking the position of two equilibria shown on the bottom-center panel.

17
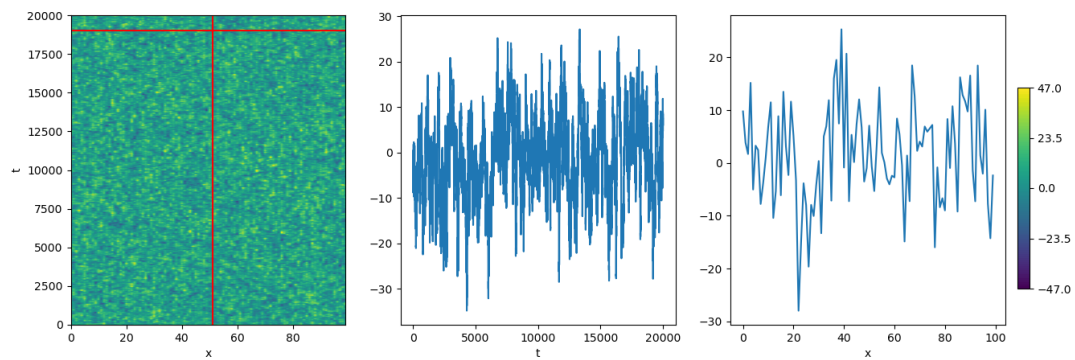
Figure A1. One ~~realisation~~ realization of the structured noise with $\sigma = 10$, $\lambda_t = 100$ and $\lambda_s = 1$. On the left panel is shown the full noise. The vertical red line and the horizontal red line mark the position of the snapshots, those snapshots are represented on the middle panel for the vertical one, and on the ~~left~~ right panel for the horizontal one.

$\sigma = 0.1$, $\lambda_t = 100.0$, $\lambda_s = 1.0$

Figure A2. Mean over 50 ~~realisations~~ realizations of the structured noise with $\sigma = 10$, $\lambda_t = 100$ and $\lambda_s = 1$. ~~One~~ On the upper-left panel, the blue line is the mean over all the ~~realisations~~ realizations with temporal autocorrelation at $t = 20000$; the orange line is the theoretical expectation. One the upper-right panel, the blue line is the mean over all the ~~realisations~~ realizations of the spatial autocorrelation at $x = 50$, the orange line is the theoretical expectation. On the bottom-left panel the blue line is the mean temporal power spectrum, and the vertical red dashed line is at $1/\lambda_t$. On the ~~bottom-left~~ bottom-right panel the blue line is the mean spatial power spectrum and the vertical red dashed line is at $1/\lambda_s$.